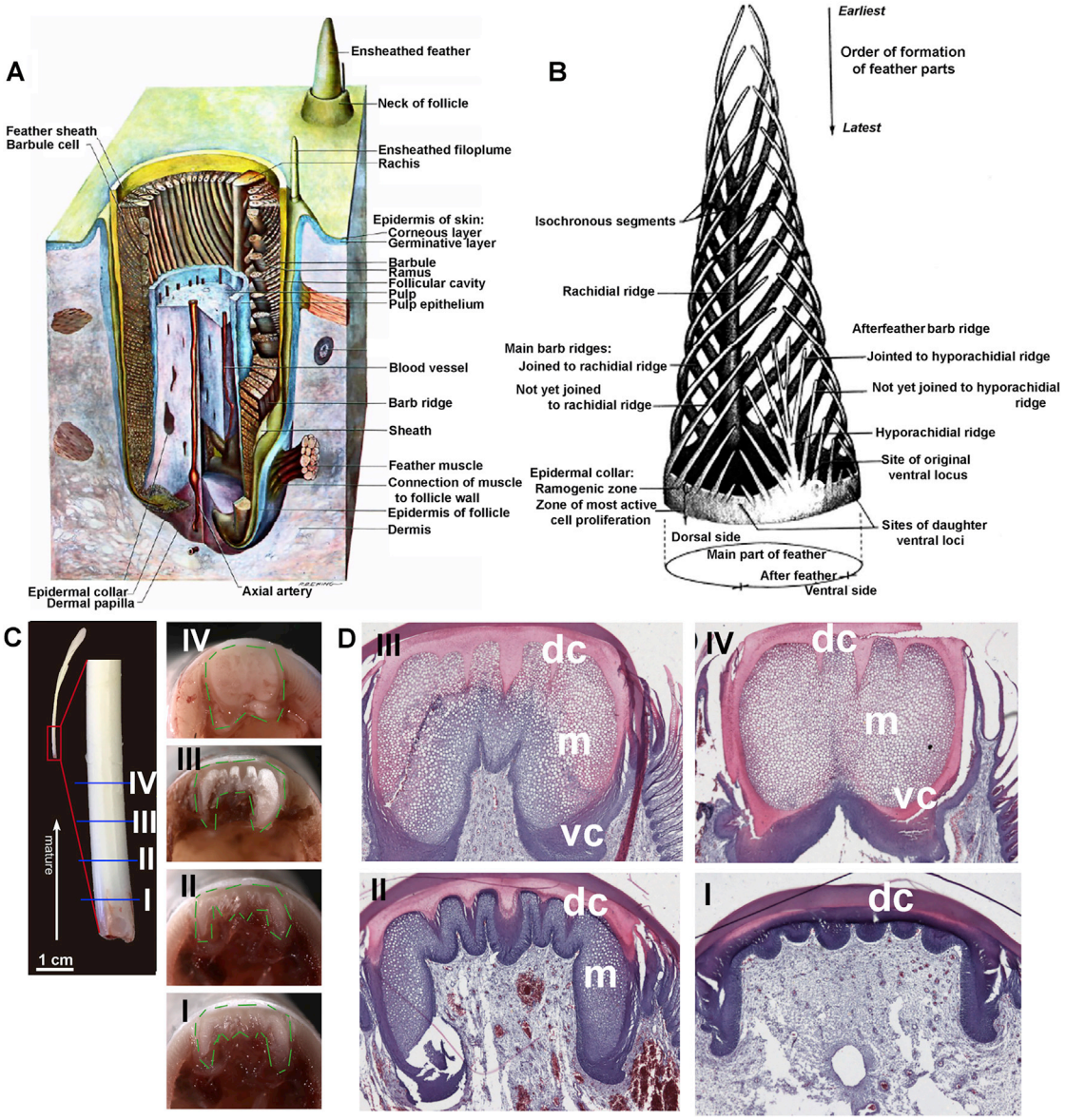

Figure S1. Topology of Feather Follicle and Cellular Organization of the Rachis, Related to Figure 1

(A) Three-dimensional view of a growth phase feather follicle (Lucas and Stettenheim, 1972).

(B) Feather branches before a feather opens. No barbules are present (Lucas and Stettenheim, 1972).

(C) A chicken flight feather in the growth phase. Serial sections in 1 cm intervals are prepared. Green dashed line indicates the shape of the rachis.

(D) H&E staining showing the development of rachis.

(dc, dorsal cortex: m, medulla; vc, ventral cortex)

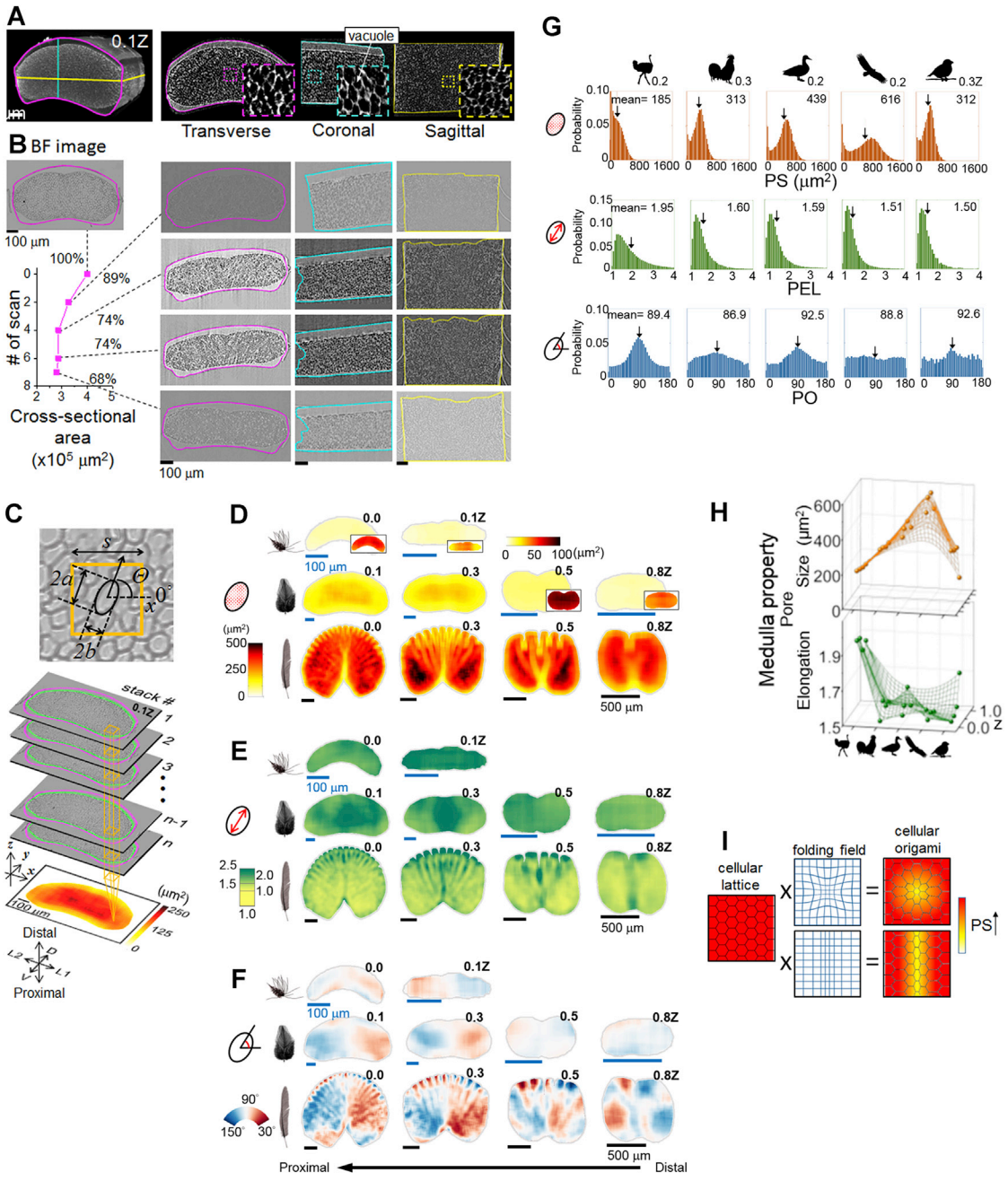

Figure S2. Morphological Characterizations of the Feather Rachis and Evaluation by QMorF (Quantitative Morphological Field) Analyses, Related to Figure 2

(A) Synchrotron X-ray micro-CT of the contour feather rachis. The 3D reconstruction of a chicken contour feather rachis near the proximal end. Three orthogonal optical sections highlighted in magenta, yellow and cyan are shown on the right panel. X-ray tomography reveals that the rachis is a composite beam with a medulla core and surrounding cortex.

(B) The rachis shrinks with increasing numbers of X-ray scans. (Left) The bright-field image (BF) of a physically sectioned rachis shows the original size of the transverse cross-section. A graph of the transverse cross-sectional area versus increasing numbers of scans shows morphological changes associated with rachis shrinkage.

(C) The q*uantitative morphology field* (QMorF) calculation. The fitted ellipse contains parameters of its major (2*a*), minor (2*b*) axes and the orientation (Θ) (upper panel). We stacked cross-sectional images aligning the *s*-by-*s* squares along the *z* axis for about 100 μm in total (marked by yellow edges). This is used to obtain mean values of pore size (PS), elongation (PEL), and orientation (PO). The schematic plot of how QMorF was measured, using PS as the example, is shown in the lower panel. QMorF results are the average of more than 8 high quality sections to ensure statistical quality.

(legend continued on next page)

(D)-(F) Comprehensive QMorF analyses of rachides from different body regions. The QMorF distributions of the PS, PEL, and PO of the rachidial medulla of chicken down, contour, and flight feathers at different positions along the *z*-axis are shown in panel (D), (E) and (F), respectively. The horizontal PS scale bar in panel D (top right), applies to the insets. The QMorF of PS, PEL (panel E) and PO (panel F) are able to illustrates distinct vacuole morphology in the rachis medulla. As shown by the third row of each panel (panels D–F), cell bands in the flight feather medulla with colocalized patterns in PS, PEL, and PO are the proposed products of cellular origami (Figure S2I). As the vacuoles represent dehydrated residues of the interconnected medullar keratinocytes, the patterned deformation of the vacuole network reflects coherently introduced mechanical stress during rachis development. Varying spatial-temporal QMorF patterns in the medulla uncovered complex region-specific variations in rachis morphogenesis.

(G) PS, PEL, and PO distributions in flight feather shafts of five different avian species. The mean value is labeled on top of each histogram and its location within the distribution is indicated by the black arrow. As demonstrated by the ostrich and chicken, the PS and PEL are narrowly distributed yet the PO is more random in the chicken than in the ostrich. These 3 parameters collectively characterize the cell band. The concise bi-laterally symmetric QMorF patterns in the ducks and eagles are composed of the larger PS, with less significant elongation and orientation.

(H) Pore size and elongation derived from different species' rachidial medullas demonstrate various degrees of cellular origami, suggested by variations in the mean of PS and PEL.

(I) The cellular lattice exhibits cellular origami under the influence of the folding field. An ideal cellular lattice subjected to various folding fields results in the cellular origami and contributes the inhomogeneous morphological field of cells.

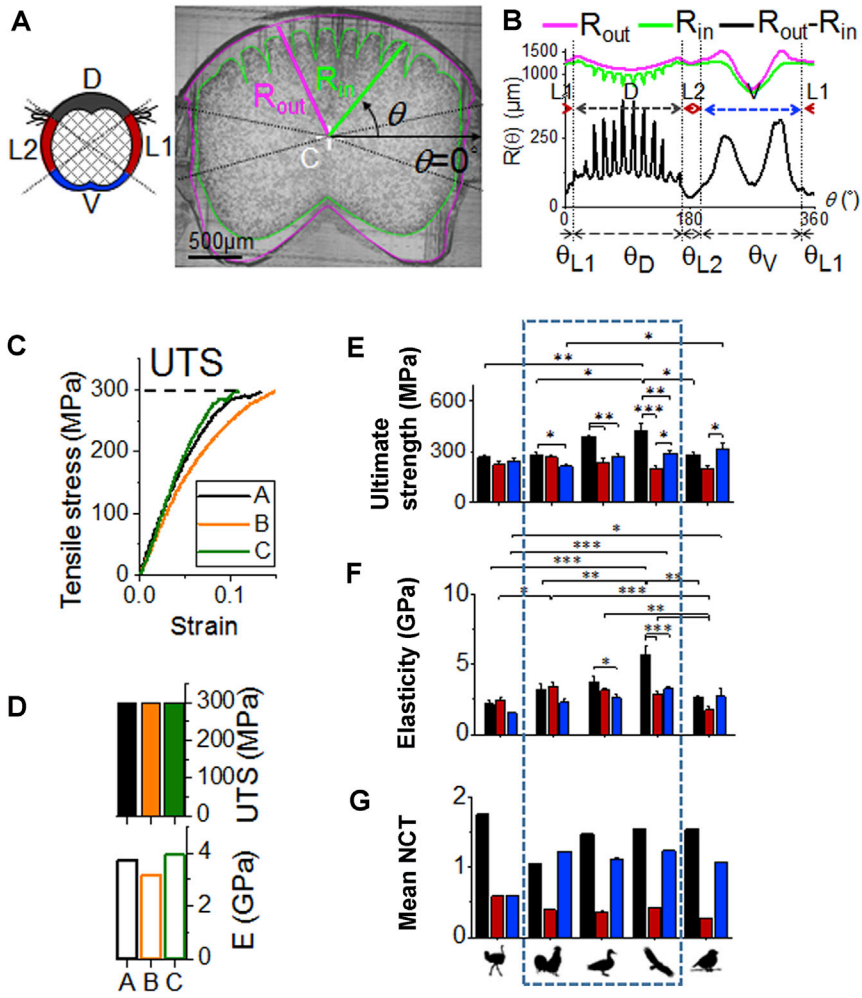

Figure S3. Functional Characterization of Rachis Properties, Related to Figure 2

(A) Regional geometric characterization of the cortex. The cortex cylinder was divided into four distinct regions, the dorsal (D), ventral (V), and two lateral cortical walls (L1 and L2) which define the lateral cortex on each side of the rachis, with polar coordinates, as illustrated by the right panel. The green line surrounds the medulla and the magenta line surrounds the rachis.

(B) Measurements of normalized regional cortex thickness. The contour of the rachis cortex is described by the radius from the geometric center to the inner R_{in} and outer cortex surfaces R_{out} in (A). The regional mean *normalized cortex thickness* (NCT) defined as $\left[2\pi \int_{\theta_i} (R_{out} - R_{in}) d\theta\right] \Big/ \left[\theta_i \int_{2\pi} (R_{out} - R_{in}) d\theta\right]$, where θ_i stands for the angular span of cortex region *i*, provides a base to compare the regional cortex thickness in a feather rachis regardless of its physical size.

(C) The force-displacement curves of the specimens, using the chicken flight feather cortex as an example, were converted to stress-strain curves.

(D) The measured ultimate tensile strength (UTS) and elastic modulus (*E*), shown in upper and lower panels, respectively, were calculated from (C).

(E) and (F) Comparison of the regional cortex properties among the five avian species. UTS and *E* of the regional cortex near proximal shafts (< 0.3Z) contributes to material rigidity. Colors in the chart correspond to the different cortex regions in the illustration in the left panel of (A).

(G) Geometric characterization of the regional cortex (D, L, V) and medulla (M) near proximal shafts (< 0.3Z) using the mean NCT. Data framed within the dashed line in (E)-(G) supports the dorsal-ventral cortex polarization, i.e., the thickening and strengthening of the dorsal and ventral cortex, and thinning and weakening of the lateral cortex.

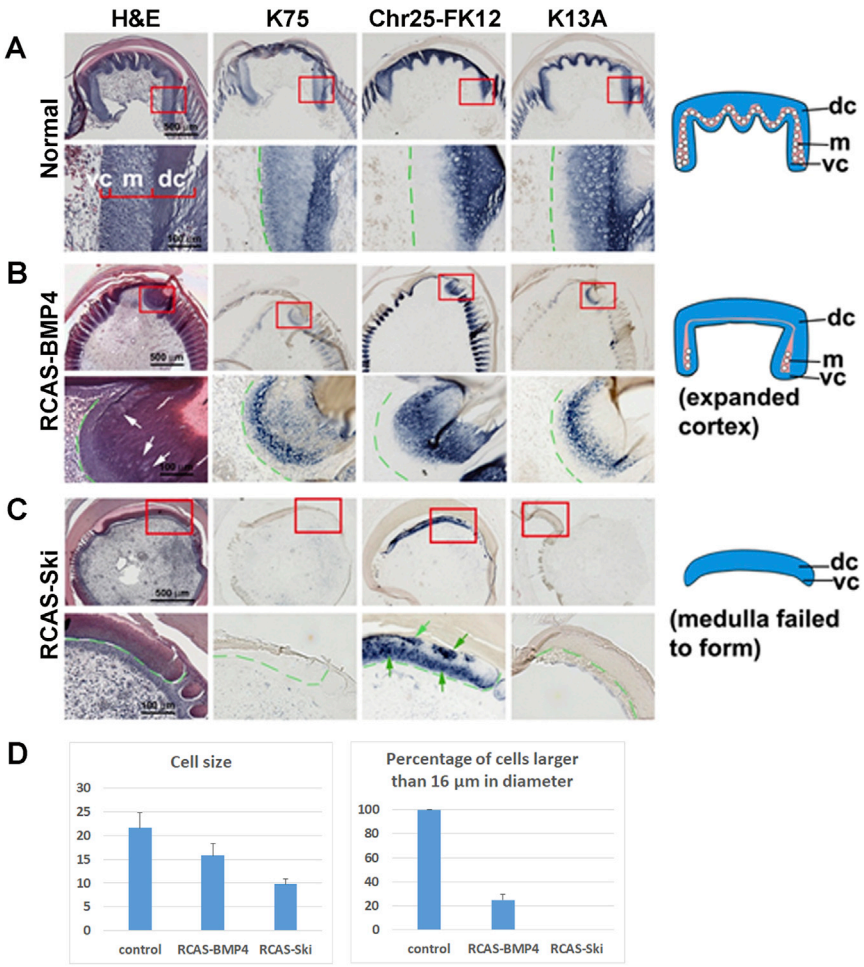

Figure S4. Molecular Perturbation Studies Leading to Unbalanced Rachis Formation, Related to Figure 3

(A-C) Paraffin sections of regenerating flight feathers were examined after 3 weeks of regeneration. (A) Normal control. (B) RCAS-*BMP4*. (C) RCAS-*Ski*. First column, H&E staining. Second to fourth columns, *in situ* hybridization of *K75*, *Chr25-FK12* and *K13A*, respectively. White arrows in B, H&E staining, indicate the reduced medulla cell formation and expanded cortex. Green arrows in C, *Chr25-FK12 in situ* hybridization indicate disrupted feather keratin expression. Green dotted lines indicate the rachis – pulp border. The schematic drawings show the phenotype after ectopic gene expression. (D) Left panel, measurement of medulla cell diameter (in the unit of μm). Right panel, percentage of medulla cells greater than 16 μm.

(*Chr25-FK12*, chromosome 25-feather keratin 12; dc, dorsal cortex; H&E, haemotoxylin and eosin; *K13A*, keratin 13A; *K75*, keratin 75; m, medulla; RCAS, replication competent avian sarcoma virus; vc, ventral cortex)

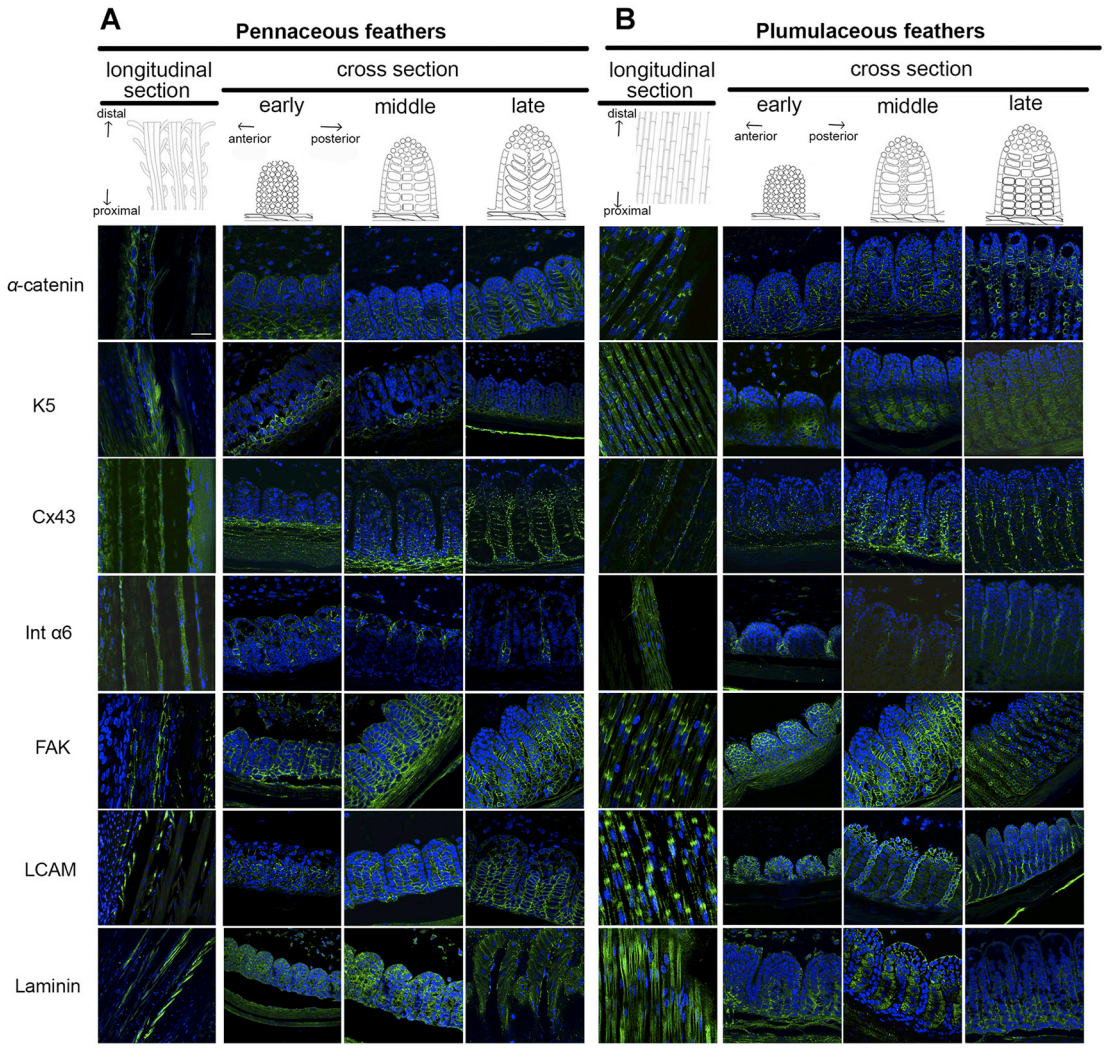

C

Morphology	Pennaceous feathers										Plumulaceous feathers									
Sections	longitudinal		cross								longitudinal		cross							
	pennulum	hooklet	early	middle			late				node	Inter-node	early	middle			late			
	x	v	x	B	A	M	B	A	M		v	x	v	B	A	M	B	A	M	
				v	x	x	v	x	x					v	v	x	v	v	x	
β-catenin	x	v	v	B	A	M	B	A	M		v	x	v	B	A	M	B	A	M	
				v	v	v	v	x	x					v	v	x	v	v	x	
FAK	x	v	v	B	A	M	B	A	M		v	x	v	B	A	M	B	A	M	
				v	v	v	v	v	x					v	x	x	v	x	x	
Cytokeratin 5	v	v	x	B	A	M	B	A	M		v	v	v	B	A	M	B	A	M	
				x	x	x	x	x	x					v	x	x	v	x	x	
Cytokeratin 17	x	v	v	B	A	M	B	A	M		x	v	v	B	A	M	B	A	M	
				v	v	v	x	x	v					x	v	v	x	v	v	
DSG1	x	v	v	B	A	M	B	A	M		v	v	v	B	A	M	B	A	M	
				v	v	x	v	x	x					v	v	x	v	x	x	
Int α6	v	v	v	B	A	M	B	A	M		v	v	v	B	A	M	B	A	M	
				x	x	v	x	x	v					x	x	v	x	v	v	
LCAM	x	v	v	B	A	M	B	A	M		v	v	v	B	A	M	B	A	M	
				v	v	x	v	v	x					x	v	v	x	v	v	
Laminin	x	v	v	B	A	M	B	A	M		x	v	v	B	A	M	B	A	M	
				v	v	v	v	x	x					v	x	x	v	x	x	
Cx43	x	v	v	B	A	M	B	A	M		x	v	v	B	A	M	B	A	M	
				v	v	v	v	v	v					v	v	v	v	v	v	

(legend on next page)

Figure S5. Molecular Characterization of Barb Ridge Morphogenesis in Pennaceous and Pulumulaceous Feathers, Related to Figure 4

(A-B) Distinct molecular expressions in barb ridges during pennaceous (A) and plumulaceous (B) barb morphogenesis. The expression patterns of α-catenin (α-cat), cytokeratin 5 (K5), connexin 43 (CX43), integrin α6 (Int α6), focal adhesion kinase (FAK), liver cell adhesion molecules (LCAM), and laminin are shown in longitudinal and cross-sections in pennaceous or in plumulaceous feathers. In cross-sections, we define early, middle, and late stages to illustrate the dynamic change of each molecule during development. (C) Summary of dynamic adhesion molecule distribution and keratinocyte assembly in pennaceous and plumulaceous feather barb branches. Bar: 15 μm.

B, barbule plate cells; A, axial plate cells; M, marginal plate cells; ˇ, signal can be detected in cells; x, signal is not or is weakly detected in cells.

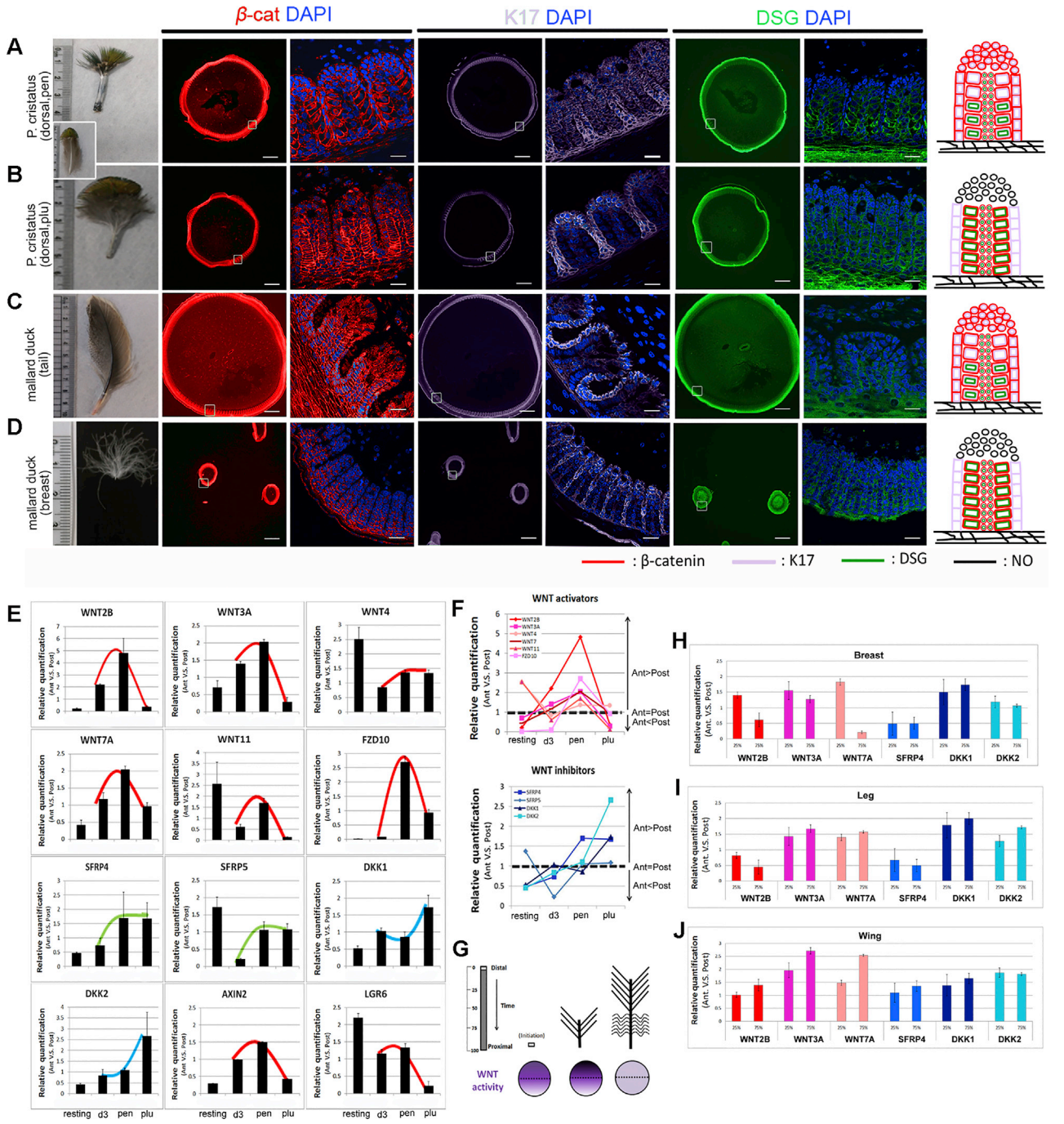

Figure S6. Further Molecular Characterization of Barb Ridge Formation in Different Birds with a Close Examination of Asymmetric WNT Signaling Activity in the Chicken Dermal Papilla Complex, Related to Figure 5

(A-D) Temporal regulation of activated WNT signaling and pennaceous/plumulaceous branch morphology is also observed in different avian species. In P. cristatus, dorsal feathers (A) display distal pennaceous and proximal plumulaceous morphologies. β-cat is expressed in all barb cells in pennaceous follicles but is exclusively expressed in barbule plate cells in plumulaceous feathers (B). K17 is expressed in all barb cells during pennaceous feather formation, but is restricted mainly to the marginal plate and slightly within axis plate cells in plumulaceous feathers. In mallard ducks, pennaceous tail (C) feathers and plumulaceous breast feathers (D) show unique β-cat and K17 expression, similar to that seen in chicken feathers in these regions. Samples were stained using Alexa Fluor 488 and then pseudocolored red (β-cat) and purple (K17) using photoshop. Images showing DSG1 staining kept the original green color. In the schematic diagram, cells expressing these molecules were indicated by using the same colors. If these three molecules are not expressed, cells in the diagram are drawn in black. When molecular expression overlaps, it is indicated in the schematic diagram with two adjacent colors. Bar: 15 μm.

(legend continued on next page)

(E) Quantitative real-time PCR shows the dynamic expression level of multiple WNT signaling related molecules in the chicken dermal papilla complex (anterior versus posterior) during resting phase, initiation phase (day three after plucking), pennaceous growing phase (time differs among feather types; day 7 in this case), and plumulaceous growing phase (day 21 in this case). The relative quantification values of each molecule are compared with GAPDH in their corresponding regions.

(F) Diagram shows the trend of WNT signaling during different developmental stages of chicken contour feathers. The dotted line (relative quantification = 1) indicates the same relative quantity of molecules between anterior and posterior regions of the dermal papilla complex.

(G) Schematic drawing to summarize the activation of WNT signaling during feather development.

(H-J) Dynamic expression of WNT signaling related molecules in the chicken dermal papilla complex.

Quantitative real-time PCR shows the relative amounts of each molecule compared to GAPDH in the breast (H), leg (I) and wing (J). Dermal papilla complexes were examined at times when 25% and 75% of the full feather length was achieved.

Ant, anterior; D3, Day 3; pen, pennaceous; plu, plumulaceous; post; posterior.

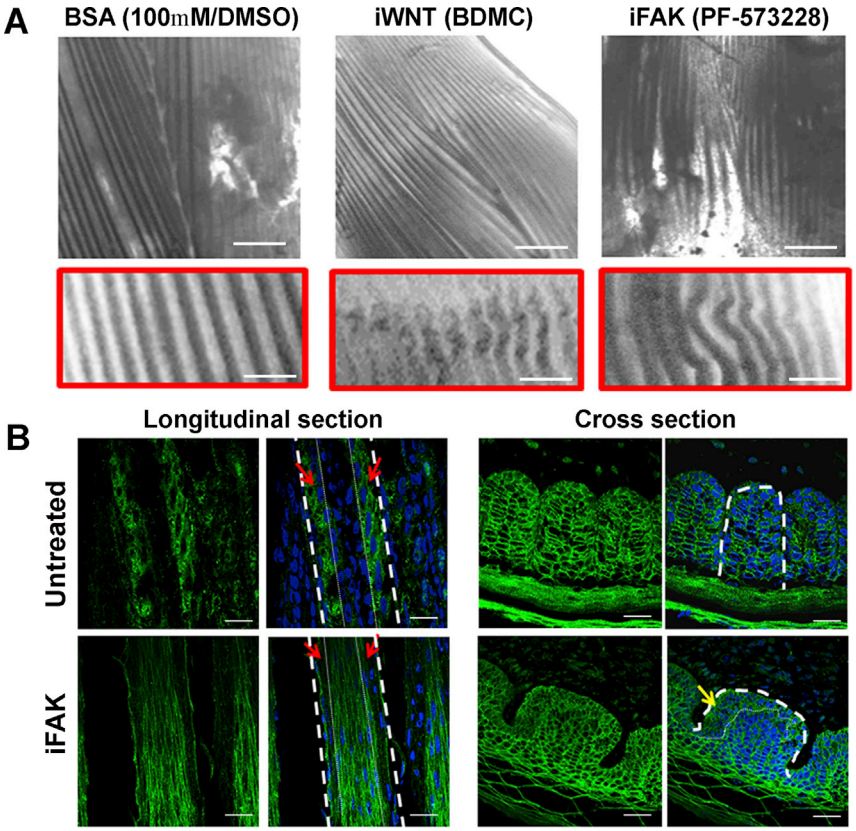

Figure S7. Molecular Perturbation Studies Leading to Loss of Vane-Forming Barbules, Related to Figure 5

(A) WNT and FAK signaling regulate barbule formation. The effects of WNT pathway and FAK disruption with specific inhibitors on pennaceous feather branch morphology. Upper panels show increasing branching occurs within the feather vane after treatment. Bar: 200 μm. Lower panels show the disturbed branch under higher magnification. Bar: 50 μm.

(B) FAK signaling regulates barbule formation. A longitudinal section shows that β-cat expression, a marker of barbule hooklet-like cells (red arrow), is reduced. A cross-section shows that the marginal plate cells have increased proliferation (yellow arrow), and the number of barbule cell rows is increased. The white dashed line indicates a barb in longitudinal section and barb ridge in cross-section. Bar: 15 μm.

(BDMC, Bisdemethoxycurxumin; BSA, bovine serum albumin; DMSO, dimethyl sulfoxide; DSG1, desmoglein 1; iFAK, focal adhesion kinase inhibitor)